



**Effect of Graphene and Au@SiO<sub>2</sub> core-shell nano-composite on photoelectrochemical performance of dye-sensitized solar cells based on N-doped titania nanotubes**

Journal:	<i>RSC Advances</i>
Manuscript ID	RA-ART-07-2015-013799.R1
Article Type:	Paper
Date Submitted by the Author:	07-Sep-2015
Complete List of Authors:	Chandrasekhar, Pakanati; IIT Delhi, Centre for Energy Studies Komarala, Vamsi; Indian Institute of Technology, Centre for Energy Studies
Subject area & keyword:	

**Effect of Graphene and Au@SiO<sub>2</sub> core-shell nano-composite on photoelectrochemical performance of dye-sensitized solar cells based on N-doped titania nanotubes**

P. S. Chandrasekhar\* and Vamsi K. Komarala

Centre for Energy Studies, Indian Institute of Technology Delhi, New Delhi-110016, India

**Abstract**

We have investigated the role of graphene and Au@SiO<sub>2</sub> core-shell nano-composite (NC), on the performance of dye-sensitized solar cells (DSSC) based on nitrogen doped TiO<sub>2</sub> nanotubes (N-TNTs) as photoanodes. The N-TNTs were synthesized by an environment-conscious solvothermal method. The photoelectrochemical performance of DSSCs with N-TNTs improved compared to undoped TNTs; due to an extended absorption in the visible part of solar spectrum. An improved open circuit voltage was also observed with N-TNTs due to change in TiO<sub>2</sub> Fermi energy level with increased electron density. After that, we investigated DSSC performance using graphene in N-TNTs with varying concentration from 0.2 to 1.0wt %. With an optimal concentration of graphene (0.6wt %), we have achieved 6.33% energy conversion efficiency, which is ~47.5 % enhancement in performance compared to pure N-TNTs. The enhanced device performance with graphene is mainly due to better dye loading, improved electron transport and charge collection process. To further boost conversion efficiency of DSSC based on graphene/N-TNTs NC, we introduced Au@SiO<sub>2</sub> core-shell nanoparticles (NPs) of different concentration in the device structure. Finally, we are able to fabricate DSSC having energy conversion efficiency of 7.01% with 1.8% (w/w) of Au@SiO<sub>2</sub> NPs, due to an improved excitation of dye molecules by generated strong near-fields around Au NPs along with incident light far-fields.

**Keywords:** N-doped TiO<sub>2</sub> nanotubes, graphene, Au@SiO<sub>2</sub> core-shell nanoparticles, dye-sensitized solar cell.

Corresponding author: Tel. 0(+91)11-2659-1255; fax. 0(+91)11-2659-1251.  
E-mail: pschandrasekhar9@gmail.com, vamsi@iitd.ac.in

## 1. Introduction

Dye sensitized solar cell (DSSC) consists of a dye adsorbed nanocrystalline  $\text{TiO}_2$  photoanode, redox-electrolyte, and a counter electrode. Over a decade, many efforts have been made for improving the electron transport, and for reducing charge carrier recombination by replacing the  $\text{TiO}_2$  nanoparticles (NPs) with 1-D  $\text{TiO}_2$  nanostructures such as nanowires, nanorods, nanotubes and nanofibers.<sup>1-4</sup> These 1-D nanostructures exhibit less grain boundaries compared to  $\text{TiO}_2$  NPs, and provide direct pathways for electron transportation, reduced charge carrier recombination.<sup>5</sup> However, with these 1-D nanostructures, till now unable to achieve appreciable energy conversion efficiencies ( $\eta$ ) (>10%) due to their less internal surface area, resulting reduced amount of dye adsorption.

The nano-composite (NC) materials are extensively used for various applications including DSSC as a scientific curiosity and for sustainable solar energy conversion. The NCs in case of DSSC can contribute enhanced adsorption of dye, light trapping as well as for efficient charge transport. To enhance the performance of 1-D nanostructures based DSSC, several attempts were also made by the researchers to engineer the active photoanode with various NC materials. Initially researchers were tried to dope metal ions (Nb, Ru and La) in  $\text{TiO}_2$  nanotubes (TNTs) to enhance the electron conductivity, and to minimize charge carrier recombination for obtaining better device efficiencies.<sup>6-8</sup> Even the incorporation of graphene (and its derivatives) in  $\text{TiO}_2$  NPs network was considered for DSSC, due to its outstanding properties like electron mobility,<sup>9</sup> and large surface area ( $\sim 2600 \text{ m}^2 \text{ g}^{-1}$ ),<sup>10</sup> for enhancing dye adsorption, and electronic conductivity.<sup>11-13</sup> Recently, Wang et al., used nitrogen-doped  $\text{TiO}_2$ /graphene NC as a low cost counter electrode instead of platinum for DSSC.<sup>14</sup> In an another approach, attempts have been made to boost  $\eta$  of DSSC based on 1-D  $\text{TiO}_2$  by utilizing plasmonic metal nanostructures in core and core-shell forms.<sup>15, 16</sup> Metal nanostructures can increase light harvesting efficiency in a device with strong confined near-

fields around metal NPs, and also resonance energy transfer from metal NPs to surrounding dye molecules.<sup>17, 18</sup>

In this study, we systematically explored effect of graphene and Au@SiO<sub>2</sub> core-shell NPs for obtaining better  $\eta$  of DSSC based on N-TNTs as photoanodes. It is known that pristine TiO<sub>2</sub> nanostructures will have some oxygen deficiency in their crystal structure, it will generate electron-hole pairs, the oxidizing holes can react either with dye molecules or scavenged by iodide ions.<sup>19</sup> So, initially we fabricated DSSC based on N-TNTs by replacing oxygen deficiency with visible light active nitrogen dopant in TNTs to improve  $\eta$  compared to pristine TNTs. Then, the effect of graphene in N-TNTs is investigated for the first time to evaluate DSSC performance. Finally, we embedded Au@SiO<sub>2</sub> NPs in optimized graphene/N-TNTs NC, to exploit surface plasmon resonances (SPRs) for attaining better efficiency with enhanced absorption process in dye molecules.

## 2. Experimental

### 2.1. Preparation of Graphene/N-TNT composites

Initially, pristine TNTs are prepared through an alkaline hydrothermal method,<sup>20</sup> and N-TNTs are prepared by an environment-conscious procedure.<sup>21</sup> In brief the preparation of N-TNTs; as prepared TNTs were well dispersed in 1:1 volume ratio of ethanol-water solution containing 20 wt. % of NH<sub>4</sub>Cl, then transferred to a Teflon-lined stainless steel autoclave, and kept in an oven at 120°C for 5 h. The obtained precipitates were washed with DI water and ethanol sequentially several times then dried at 60°C overnight, finally calcined at 400°C for 2 h. The same procedure was repeated for preparation of graphene/N-TNT NCs by introducing graphene in reaction solution with different weight ratio of 0.2%, 0.4%, 0.6%, 0.8% and 1.0%.

## 2.2. Synthesis of Au@SiO<sub>2</sub> Core-Shell NPs.

Au NPs were synthesized according to the standard sodium citrate method (Enustun et al., 1963),<sup>22</sup> and Au@SiO<sub>2</sub> core-shell NPs were synthesized by following two step procedure (Graf et al., 2003).<sup>23</sup> In brief, an aqueous polyvinyl pyrrolidone (10 kg/mol.) solution was added to the 30 ml of as prepared Au NPs solution, stirred for 24 h at room temperature, centrifuged at 10000 rpm, and the obtained sediment was redispersed in a solution of 4.2 vol. % ammonia in ethanol. Immediately, tetraethoxysilane (10 vol. % in ethanol) solution was added, and kept the reaction mixture stirring for 12 h.

## 2.3. Preparation of graphene/N-TNT composite and Au@SiO<sub>2</sub> NPs embedded composite pastes.

As prepared graphene/N-TNT NCs were well dispersed in ethanol by an ultra-sonication for 1 h, and concentrated with a rotary-evaporator to remove excess solvent. The obtained product was smoothly grinded in a mortar pestle by adding 1 mL of glacial acetic acid, and 40 wt.% aqueous polyethylene glycol solution drop wise (to increase the connectivity among TNTs) to obtain a thick paste. The Au@SiO<sub>2</sub> NPs with different concentrations varying from 0.6 to 2.4 wt% embedded in graphene/N-TNT NCs paste was also prepared by the similar procedure.

## 2.4. DSSC Assembly

Fluorinated tin oxide (FTO) conductive glass substrates were used as working and counter electrodes. Substrates were cleaned with a detergent, and sonicated in solution of DI water, isopropanol, and acetone (1:1:1 vol. ratio) for 1 h. A compact TiO<sub>2</sub> thin layer (~80 nm) was deposited on FTO coated glass substrate by aerosol spray pyrolysis method at 450°C temperature, the spray solution was prepared from titanium di-isopropoxide *bis*-(acetylacetonate) in ethanol (1:9 Vol. ratio). As prepared pastes of different weight ratios of graphene/N-TNT NCs were made into thin films having thickness of ~10 μm on FTO

substrates by using doctor-blade method. Initially air dried for some time, then annealed at 450°C for 30 min, followed by TiCl<sub>4</sub> treatment at 70°C for 30 min, and further annealed at 450°C for 30 min. For dye sensitization, prepared photoanodes were immersed in a 0.5 mM N719 dye dissolved ethanol solution for 24 h, and the same procedure was repeated for plasmonic photoanodes having thickness of ~6 μm with Au@SiO<sub>2</sub> NPs embedded in graphene/N-TNT NC paste. The platinum coated counter electrode (DC sputtered on FTO glass substrate) and as prepared photoanodes were assembled by introducing a liquid electrolyte (0.05 M LiI, 0.05 M I<sub>2</sub>, DMPI, and 0.5 M *tert*-butylpyridine in acetonitrile) to prepare DSSCs. The DSSC structure based on N-TNTs, graphene, and Au@SiO<sub>2</sub> NPs is shown in Scheme 1. In practicality, the dye adsorption occurs over entire photoanode, here in schematic for easy understanding, we have represented an attachment of dye molecules over composite materials as a red spheres.

## 2.5. Characterization of samples/devices

X-ray diffraction patterns were recorded using a Rigaku Ultima IV diffractometer (Japan) with Cu K $\alpha$  radiation ( $\lambda = 1.5406\text{\AA}$ ) as a source. Transmission Electron Microscopy (TEM) images were obtained using a Technai G<sup>2</sup> (USA) high resolution TEM instrument operated at 200 kV. Scanning Electron Microscopy (SEM) images were obtained from Carl Zeiss, EVO-18 microscope. X-ray photoelectron spectroscopy (XPS) analysis was carried out by using SPECS instrument having Mg K $\alpha$  radiation source for X-rays. Absorbance spectra were recorded by using Perkin Elmer Lambda (1050) UV-Vis-NIR spectrophotometer. Photocurrent density-voltage (J-V) characteristics of DSSC were recorded from an active area of 0.25 cm<sup>2</sup> by using solar simulator (Oriel sol 3A) from Newport Corporation under an illumination of one sun condition (100 mW/cm<sup>2</sup>), which is equipped with a 450 W xenon lamp, and a Keithley 2440 source meter. Incident photon to current conversion efficiency (IPCE) measurements were recorded using a SpeQuest Quantum efficiency measurement

system from ReRa solutions of The Netherlands, the Silicon photodiode was used for calibrating IPCE spectrum. IPCE measurements were recorded at incident light chopping frequency of 20 Hz, and also with the bias light intensity of 0.1 Sun. Electrochemical impedance spectra (EIS) were recorded using Zahner Zennium (Germany) system with an applied A. C. voltage of 10 mV in a frequency range from 0.1 Hz to 1 MHz, at an open circuit voltage conditions, and one sun illumination ( $100 \text{ mW/cm}^2$ ).

### 3. Results and Discussion

The XRD patterns of as prepared pristine TNTs, N-TNTs, and graphene/N-TNT composites are presented in supplementary information (SI) as Fig. S1. The observed characteristic diffraction peaks (101), (004), (200), (105), (211), (204), (116), (220), and (215) of TNTs are in well agreement with the standard anatase phase of  $\text{TiO}_2$  (JCPDS no. 21-1272). The N-TNTs and graphene/N-TNT NCs are also exhibited the same diffraction patterns as that of pristine TNTs. In case of NCs, the diffraction peaks of graphene is not visible due to very small quantity. The diffraction pattern of pure graphene is shown as an inset of the Fig. S1, which shows a sharp diffraction peak from (002) plane at  $2\theta = 26.4^\circ$ . The average crystallite sizes of pristine TNTs and N-TNTs are estimated from the (101) diffraction peak by using the Scherrer formula, which are  $\sim 16.5$  and  $\sim 17.6$  nm, respectively.

Fig. 1a shows TEM image of N-TNTs, which are open-ended nanotubes with a diameter ranging from 20 to 25 nm, having length up to several hundred nanometres ( $\sim 250$  nm). Fig. 1b shows the morphology of graphene sheets, and TEM micrographs of graphene/N-TNT NC with 0.6wt% and 1wt% graphene are shown in Fig. 1c and Fig. 1d. In case of NC, graphene sheets are well distributed over N-TNTs with 0.6wt% concentration, with the higher amounts of graphene (1.0wt %) agglomerated network of nanotubes was observed, this type of dense morphology of photoanode can affect photovoltaic performance of device, which we

discussed in detail in the following section. Fig. 1e and Fig. 1f show SEM micrographs with a large area of pure N-TNTs, and cross sectional view of 0.8wt% of graphene/N-TNT NC films, respectively.

The UV-Vis absorbance spectra of pristine TNTs and N-TNTs are shown in Fig. 2a. One can observe that N-TNTs are showing an enhanced absorption from 400 to 570 nm wavelength region as compared to pristine TNTs. It confirms that N-TNTs are photoactive in the visible region of polychromatic spectrum; with the nitrogen doping additional energy levels are introduced in the energy band gap of  $\text{TiO}_2$  for visible absorption transitions.<sup>24</sup> Inset of Fig. 2a shows estimated optical band gap of TNTs with and without nitrogen, which is found to be  $\sim 2.92$  eV for N-doped TNTs compared to pristine TNTs band gap of  $\sim 3.16$  eV. The reduction of band gap is due to the substitution of nitrogen atoms in place of oxygen vacancies, leading to the formation of O-Ti-N bond in TNTs. The digital photographs of pristine TNTs and N-TNTs powders are also presented in Fig. 2b and Fig. 2c. The N-TNTs powder is in yellow colour compared to pure TNTs having white, it gives a clear indication that N-TNTs are interacting with incident visible light, so, some part of the polychromatic spectrum is absorbed, and yellow light is scattering back from the powder. To have further microscopic electronic evidence, XPS measurements were conducted to see the modifications in electronic configuration of N-TNTs compared to pure TNTs. Fig. 3a and Fig. 3b show XPS wide scan and nitrogen 1s core level spectra of pristine TNTs and N-TNTs, respectively. One can see peak at  $\sim 398.6$  eV in the spectrum related to nitrogen bonding in TNTs in the form of O-Ti-N.<sup>25</sup> These measurements are also providing clear evidence that during synthesis some oxygen atoms are substituted with nitrogen atoms in the  $\text{TiO}_2$  lattice as intrinsic dopants.

The current density-voltage (J-V) graphs of DSSC based on pristine TNTs, N-TNTs, and graphene/N-TNT NCs are shown in Fig. 4a, and their photovoltaic parameters are summarized in Table 1. With N-TNTs, we found a small enhancement in photocurrent ( $J_{sc}$ )

and open circuit voltage ( $V_{oc}$ ) compared to pure TNTs. DSSC prepared with N-TNTs resulted  $\eta$  of 4.29% compared to DSSC with pristine TNTs shown  $\eta$  of 3.86%. The doping of nitrogen in TNTs can increase surface roughness factor, which can make the photoanode more porous for dye intake.<sup>24, 25</sup> Guo et al., also demonstrated the changes in pH dependent zeta potential and isoelectric points for nitrogen doped  $TiO_2$ , usually surfaces with higher isoelectric points are preferable for more dye adsorption on  $TiO_2$  surface,<sup>26</sup> which is also evident in our case (Fig. 4b). With graphene/N-TNT NC, we observed graphene concentration dependent significant improvement in  $J_{sc}$  and  $\eta$  as compared to N-TNTs (Fig. 4a). The optimized concentration of 0.6wt % graphene in N-TNTs NC based DSSCs exhibited  $\eta$  of 6.33% with  $J_{sc}$  of 12.86  $mA/cm^2$ ,  $V_{oc}$  of 0.715 V, and FF of 65.13% as compared to that of pure N-TNTs based DSSC has  $\eta$  of 4.29% with a  $J_{sc}$  of 8.34 $mA/cm^2$ ,  $V_{oc}$  of 0.696 V, and FF of 73.80%. This is nearly 54% photocurrent enhancement with 0.6 wt% graphene in N-TNTs compared to pure N-TNTs.

The gradual increase of graphene concentration in  $TiO_2$  nanostructures can increase the porosity, eventually the amount of dye loading will be enhanced. This is confirmed by dye desorption measurements from photoanodes of graphene/N-TNT NCs. The absorption spectra of desorbed dye molecules from photoanodes of graphene/N-TNT NCs having same thickness ( $\sim 10 \mu m$ ) and same area ( $\sim 1.5 cm^2$ ) are presented in Fig. 4b. The characteristic absorption peak at 532 nm is of N719 dye molecules, and its intensity is systematically varied with increase of graphene concentration from 0.2 to 1.0wt % in N-TNTs. The maximum absorption observed with 0.6wt% graphene/N-TNT, which confirms the maximum  $J_{sc}$  enhancement observed from the DSSC. The enhancement of  $\eta$  is mainly due to the increased dye loading (see table 1), which will generate more number of charge carriers. However, with further increase of graphene in N-TNTs, the amount of dye adsorption is reduced. The increase of graphene concentration led to the agglomeration of graphene sheets in N-TNTs

with the cracks formation in photoanode during annealing process (see Fig. 1f). Hence, the higher concentrations of graphene (0.8 and 1.0wt %) decreases the amount of dye loading, due to reduced porosity and disrupting compact structure resulted the reduced  $J_{sc}$  and  $\eta$  of DSSC.

The improvement in  $J_{sc}$  with optimized graphene concentration can also be due to some extent efficient electron transfer. The well-defined 2-D graphene sheets are good electron conductors, and the graphene network can also act as a bridge between dye and N-TNTs for faster electron transport, which can also facilitate in decrease of electron recombination process.<sup>27</sup> The other important observation is the increase of  $V_{oc}$  with nitrogen doped TNTs, and with graphene/N-TNTs NCs compared to pure TNTs. At open circuit condition, the  $V_{oc}$  represents the energy difference between Fermi energy level of  $TiO_2$  and redox potential of  $I^-/I^{3-}$  electrolyte. The Fermi energy of electrons in TNTs and redox potential of electrolyte correspond to Fermi energies of the minority and majority carriers, respectively in the DSSC. The formation of O-Ti-N bonding in N-TNTs can increase electron density at the conduction band (CB), which can lead to the shift in quasi Fermi energy level towards higher energy than the pristine TNTs. In the case of graphene/N-TNTs NCs, further enhancement of  $V_{oc}$  (see table I) is due to increase of photo-excited electrons leading to further shift in quasi Fermi energy level towards the CB of TNTs. There may be also some modification of potentials at the photo- and counter electrodes interfaces with the graphene/N-TNT NC, which can also affect the open circuit voltage of the device apart from Fermi energy and redox potentials.

To see incident wavelength dependent photocurrent enhancements, IPCE measurements were also conducted and the corresponding spectra are presented in Fig. 4c. One can see a slight improvement in photocurrent with N-TNTs in IPCE spectrum compared to pristine TNTs, which is due to the enhanced photo response of N-TNTs in the visible part of incident light spectrum. Similar observation was also made by Lindgraen et al,<sup>28</sup> where the enhanced

photocurrent was reported from nitrogen doped TiO<sub>2</sub> (prepared by using DC magnetron sputtering) as compare to undoped TiO<sub>2</sub> electrode. With the graphene/N-TNTs NC also concentration dependent photocurrent observed in IPCE spectra. The observed enhancement in IPCE is around 55% with the 0.6wt % of graphene/N-TNT NC as compared to pure N-TNTs, the observed IPCE peak around 530 nm is due to strong N719 dye molecules absorption. The IPCE mainly depends on light absorption efficiency of dye, the quantum yield of electron injection and collection efficiency at the conducting glass substrate,<sup>29</sup> these are all important steps in energy conversion process.

With the optimized graphene/N-TNTs NC based photoanode, we further explored the plasmonics concept using Au@SiO<sub>2</sub> core-shell NPs for enhancing the DSSCs efficiency. The morphology and absorption spectra of Au@SiO<sub>2</sub> NPs are shown in Fig. 5. The Au NPs are having sizes ~20 nm (figure 5a) with the strong SPR absorption peak at ~524 nm, with a ~5 nm SiO<sub>2</sub> thin shell absorption peak slightly red shifted to ~533 nm due to modified dielectric environment (spectra are recorded when the NPs are in water) (Fig. 5b). The advantages with insulating SiO<sub>2</sub> shell around Au NPs are; the shell can prevent corrosion of Au NPs by liquid electrolyte, and also inhibits the Ostwald ripening process at high temperature during device fabrication.<sup>30</sup> The TEM micrograph of Au@SiO<sub>2</sub> NPs integrated in graphene/N-TNTs NC is also presented in Fig. 5c. One can see the uniform distribution of Au@SiO<sub>2</sub> NPs throughout graphene/N-TNT NC.

The J-V graphs of DSSC prepared using Au@SiO<sub>2</sub> NPs of different concentrations (0.6, 1.2, 1.8 and 2.4 wt. %) incorporated in 0.6wt% graphene/N-TNTs NC based photoanodes are presented in Fig. 6a, their photovoltaic parameters and the amount of dye adsorption in photoanodes are summarized in Table 2. The amount of dye loading in DSSCs is decreased marginally as compared to 0.6wt% graphene/N-TNTs NC, but the performance was seen to improve due to light harvesting effects of Au@SiO<sub>2</sub> NPs. The decrease in dye loading amount is because of the presence of some Au@SiO<sub>2</sub> NPs already on the surface of

graphene/N-TNTs NC based photoanode, which decreases the overall availability of surface sites for dye molecules attachment. When the concentration of Au@SiO<sub>2</sub> NPs is increased from 0.6 to 1.8 wt%, the J<sub>sc</sub> and η of DSSC are gradually increased. The observed maximum η of 7.01% for DSSC with J<sub>sc</sub> of 15.61 mA/cm<sup>2</sup>, V<sub>oc</sub> of 0.715, and FF of 62.7% for a concentration of 1.8wt% Au@SiO<sub>2</sub> NPs in a NC, which is around 21.3% enhancement in J<sub>sc</sub>. However, with further increasing of concentration (~2.4 wt% of Au@SiO<sub>2</sub> NPs), J<sub>sc</sub> and η are decreased, because of disruption in charge transportation pathways, and also excessive Au NPs can also act as recombination sites for excited electrons, and increased light absorption by Au NPs can transform part of incident solar power into heat.<sup>31, 32</sup> The observed concentration dependent enhancement clearly shows that there should be an optimum distance between dye molecules and metal NPs for exploiting the SPRs effect.<sup>33</sup> The enhancement of J<sub>sc</sub> with Au@SiO<sub>2</sub> NPs is due to strong electromagnetic fields produced by SPRs of Au NPs around the light absorbing dye molecules. With these excited near-fields of Au@SiO<sub>2</sub> NPs near dye molecules, the generation rate of photo electrons increases with the enhanced absorption transition rate. The ~5nm silica shell around Au NPs will also prevent the direct contact with the liquid electrolyte and inhibit electron or hole tunnelling into the metal core.<sup>30</sup> In addition, we have also performed the stability measurements of high efficiency DSSCs with and without Au@SiO<sub>2</sub> NPs for 110 h, with an interval of ~12-13 h under ambient conditions after fabrication. The corresponding J-V graphs are presented in SI as Fig S2. One can observe the time dependent strong decrement of cell photovoltaic parameters (short-circuit current and open circuit voltage) in both cases. The conversion efficiency values of DSSC without Au@SiO<sub>2</sub> NPs reduced to 3.66% from 6.41% after 110 h, which is mainly because of liquid electrolyte corrosion, and may be the dye molecules detachment from photoanode, leading to the reduction in the device performance. But, the device with Au@SiO<sub>2</sub> NPs, the conversion efficiency reduced to 5.23% only from 7.16% after 110 h. So, there is a corrosion issue, but, the degradation of DSSC varied with and without Au@SiO<sub>2</sub> NPs, further investigations are required in this direction for better understanding, and for improving the stability of the device after fabrication.

We further recorded the spectral response of DSSCs fabricated with Au@SiO<sub>2</sub> NPs integrated in graphene/N-TNTs NC, the IPCE spectra are presented in Fig. 6b. The enhanced spectral response is clearly observed in the visible region of the incident light spectrum. The inset of Fig. 6b also shows the relative IPCE enhancement ( $\Delta\text{IPCE}/\text{IPCE}_{0.6\text{wt}\% \text{ G/N-TNTs}}$ ) with

Au@SiO<sub>2</sub> NPs in the NC. The broadened absorption range of light by dye molecules due to SPRs of Au NPs is clearly evident, which can stimulate the dye for generating more charge carriers. To explain the enhanced  $J_{sc}$ , Guo et al., proposed some type of Schottky barrier formation at the metal/TiO<sub>2</sub> interface, these interfaces can act as electron-hole separation centres,<sup>34</sup> which can benefit for improving movement of generated electrons passing through the graphene/TNT network quickly, but they also observed increased resistance in device structure with increase of Au NPs concentration. In our case also despite of enhancement in photocurrent, after 1.2 wt% of Au@SiO<sub>2</sub> NPs, the fill factor values of DSSC reduced gradually (see table 2). So, even with the  $\sim 3\text{mA}/\text{cm}^2$  enhancement in photocurrent with 1.8wt% of Au@SiO<sub>2</sub> NPs compared to without NPs, the improvement in the overall device conversion efficiency is small. The charge transfer mechanism in the device structure is affected with the increasing concentration of Au NPs, which is clearly reflected with the reduction of FF. It is presumable that higher concentrations of Au NPs are not uniformly distributed in graphene/N-TNTs composite, resulting in formation of clusters and bumpiness of adsorbed dye layer over photoanode. This can increase the unfavourable current shunting paths, and the deterioration of interface between graphene/N-TNT NCs and electrolyte.

These observations reveal that, the optimization of materials in composite related to optical and electrical performance improvement in device structure seems to be very complex, one material can easily influence the other functionalities like; with 1.8wt% Au@SiO<sub>2</sub> NPs enhanced optical effect (photocurrent) but reduced electrical effect (fill factor). The important task with NCs for DSSC is optimization of charge carrier recombination with the large diffusion length of charge carriers with in the non-homogeneous absorber layers of smaller thickness. Up to certain extent graphene supports enhancement in photocurrent (with enhanced adsorption of dye) by increasing surface area after folding within supporting TNTs matrix with the nearly same thickness of device, but, further increase of graphene

concentration charge carriers are not reaching the metal contact due to increased resistance in the device.

To support above observations and arguments, the impedance spectroscopy measurements are also performed for the best DSSC prepared with photoanodes from TNTs, N-TNTs, 0.6wt% graphene/N-TNT NCs, and 1.8wt% Au@SiO<sub>2</sub> core-shell NPs incorporated NC, the spectra are presented in Fig. 7. As one can see in Nyquist plots (Fig. 7a), the charge carrier recombination resistance gradually increased from TNTs to the Au@SiO<sub>2</sub>NPs/0.6wt% graphene/N-TNTs. The incorporation of nitrogen into TiO<sub>2</sub> matrix can increase the surface resistance of photoanodes, and can suppress the back transfer of electrons to the interface of N-TNTs/dye/electrolyte. The graphene in N-TNTs can also act as bridging layer which helps in effective separation and transport of photo generated electrons from CB of TiO<sub>2</sub>, thereby efficiently separating the electrons and preventing charge carrier recombination through “hopping-bridging mechanism”.<sup>35</sup> The increased recombination resistance in plasmonic devices is attributed to the suppression of electron recombination by insulating thin SiO<sub>2</sub> shell. So, shell can hinder the carrier trapping and recombination apart from preventing corrosion of Au NPs with redox electrolyte (I<sup>-</sup>/I<sub>3</sub><sup>-</sup>). In bode plots (Fig. 7b) the introduction of graphene and Au NPs into N-TNTs shifts the mid frequency peak slightly to lower frequencies, which basically represents the modified charge carrier lifetimes. The charge carrier life time values are estimated by using the relation of  $\tau_e = 1 / (2\pi f_{\max})$ , where  $f_{\max}$  is the maximum point of middle frequency peak, and the estimated charge carrier lifetime values are 22.4 ms for the case of pristine TNTs, ~28.6 ms for N-TNTs, ~39.4 ms for 0.6wt% graphene/N-TNT NCs, and ~42.3 ms for Au@SiO<sub>2</sub> core-shell NPs integrated in graphene/N-TNT NCs. There is a consistent increase of charge carrier lifetimes with the corresponding enhancement in photocurrent from pure TNTs to Au@SiO<sub>2</sub> NPs incorporated NC.

The effective carrier lifetimes in NC can be considered as local surface recombination of electrons, it gives an idea of the injected electrons in CB of TNTs either back transfer to charged dye molecules or by reducing the species in the electrolyte. Initially the recombination of electrons or diffusion is retarded by fast trapping of electrons within the distributed trap states near the CB of TNTs. The detrapping times may be longer for the nitrogen doped TNTs due to additional trap states, the traps occupied with electrons can affect carrier lifetimes. With graphene skeleton, the improved lifetime value also shows some type of surface passivation, and improved transport process, which is an indication of reduced dark current generation from the excited charge carrier recombination either with triiodide ions or/and with the excited dye molecules at the TNTs/dye/electrolyte interface. Electron lifetimes also become longer with Au NPs, which indicates that the recombination rate of the CB electrons is hindered significantly due to schottky barriers formation at the Au-graphene/N-TNTs NC interface.<sup>34</sup>

#### 4. Conclusions

In Summary, we have investigated systematically the photoanodes of DSSC prepared with NCs using N-TNTs, graphene and Au@SiO<sub>2</sub> core-shell NPs for enhancing the device performance. Results indicate that N-TNTs demonstrated better performance as compared to pristine TNTs due to an increased surface roughness factor led to increased dye loading. With graphene/N-TNT NCs, we have observed functionalities like enhanced dye adsorption and to some extent improved charge transport. An enhancement of Voc in N-TNTs and graphene/N-TNTs, is because of synergic effects of reduced recombination and increased electron density, resulting modifications in quasi Fermi energy level of TNTs. The observed improvement in photocurrent with Au NPs is due to the enhanced light absorption by the dye molecules in the vicinity of strong near-fields of NPs.

## Acknowledgements

One of the authors (P.S. Chandrasekhar) would like to thank Department of Science and Technology (DST), Govt. of India for granting fellowship under DST INSPIRE Fellowships (Code No. IF-120755) programme. Authors also would like to acknowledge the funding from DST, Govt. of India, under Solar Energy Enabling Research grant number RP02914. Authors also thank Mr. Akshay Khasul for TEM analysis.

## References

1. X. Feng, K. Shankar, O. K. Varghese, M. Paulose, T. J. Latempa and C. A. Grimes, *Nano Lett.*, 2008, **8**, 3781–3786.
2. H. S. Kim, Y. J. Kim, W. Lee and S. H. Kang, *Applied Surface Sci.*, 2013, **273**, 226–232.
3. K. Zhu, N. R. Neale, A. Miedaner and A. J. Frank, *Nano Lett.*, 2007, **7**, 69–74
4. A. S. Nair, R. Jose, Y. Shengyuan and S. Ramakrishna, *J. Colloid and Inter. Sci.*, 2011, **353**, 39–45.
5. S. P. Albu, A. Ghicov, J. M. Macak, R. Hahn and P. Schmuki, *Nano Lett.*, 2007, **7**, 1286–1289.
6. M. Yang, D. Kim, J. Himendra, K. Lee, P. Jonathan and P. Schmuki, *Chem. Commun.*, 2011, **47**, 2032–2034.
7. S. So, K. Lee and P. Schmuki, *Physica Status Solidi: Rapid Research Lett.*, 2012, **6**, 169–171.
8. S. Subha and P. Pankaj, *RSC Adv.*, 2013, **3**, 10363-10369.
9. X. Du, I. Skachko, A. Barker and E. Y. Andrei, *Nat. Nanotechnol.*, 2008, **3**, 491–495.
10. A. Peigney, C. Laurent, E. Flahaut, R. R. Bacsa and A. Rousset, *Carbon* 2001, **39**, 507–514.
11. N. Yang, J. Zhai, D. Wang, Y. Chen and L. Jiang, *ACS Nano*, 2010, **4**, 887-894.

12. X. Fang, M. Li, K. Guo, Y. Zhu, Z. Hu, X. Liu, B. Chen and X. Zhao, *Electrochim. Acta*, 2012, **65**, 174-178.
13. H. Wang and Yu. H. Hu, *Energy Environ. Sci.*, 2012, **5**, 8182-8188.
14. R. Wang, Q. Wu, Y. Lu, H. Liu, Y. Xia, J. Liu, D. Yang, Z. Huo and X. Yao, *ACS Appl. Mater. Inter.*, 2014, **6**, 2118-2124.
15. R. A. Naphade, M. Tathavadekar, J. P. Jog, S. Agarkar and S. Ogale, *J. Mater. Chem. A*, 2014, **2**, 975-984.
16. G. Sahu, S. W. Gordon and M. A. Tarr, *RSC Adv.*, 2012, **2**, 573-582.
17. X. Dang, J. Qi, M. T. Klug, P. -Y. Chen, D. S. Yun, N. X. Fang, P. T. Hammond and A. M. Belcher, *Nano Lett.*, 2013, **13**, 637-642.
18. Q. Wang, T. Butburee, X. Wu, H. Chen, G. Liu and L. Wang, *J. Mater. Chem. A*, 2013, **1**, 13524-13531.
19. M. Mrowetz, W. Balcerski, A. J. Colussi and M. R. Hoffmann, *J. Phys. Chem. B*, 2004, **108**, 17269-17273.
20. C. C. Tsai, and H. S. Teng, *Chem. Mater.*, 2004, **16**, 4352-4358.
21. Z. Jiang, F. Yang, B. T. T. Luo Chu, D. Sun, H. Shi, T. Xiaoa and P. P. Edwards, *Chem. Commun.*, 2008, **47**, 6372-6374.
22. B. V. Enustun and J. Turkevich, *J. Am. Chem. Soc.*, 1963, **85**, 3317-3328.
23. C. Graf, D. L. V. Vosse, A. Imhof and A. V. Blaaderen, *Langmuir*, 2003, **19**, 6693-6700.
24. J. Zhang, Q. Sun, J. Zheng, X. Zhang, Y. Cui, P. Wnag, W. Li and Y. Zhu, *J. Renewable and Sustainable Energy*, 2011, **3**, 033108-(1)-033108-(9).
25. T. Ma, M. Akiyama, E. Abe and I. Imai *Nano Lett.*, 2005, **5**, 2543-2547.
26. W. Guo, Y. Shen, L. Wu, Y. Gao and T. Ma, *J. Phys. Chem. C*, 2011, **115**, 21494-21499.
27. Y. H. Ng, I. V. Lightcap, K. Goodwin, M. Matsumura and P. V. Kamat, *J. Phys. Chem. Lett.*, 2010, **1**, 2222-2227.
28. T. Lindgraen, J. M. Mwabora, E. Avendano, J. Jonsson, A. Hoel, C. Granqvist and S. Lindquist, *J. Phys. Chem. B*, 2003, **107**, 5709-5716.
29. Q. Wang, J. E. Moser and M. Grätzel, *J. Phys. Chem. B*, 2005, **109**, 14945-14953.

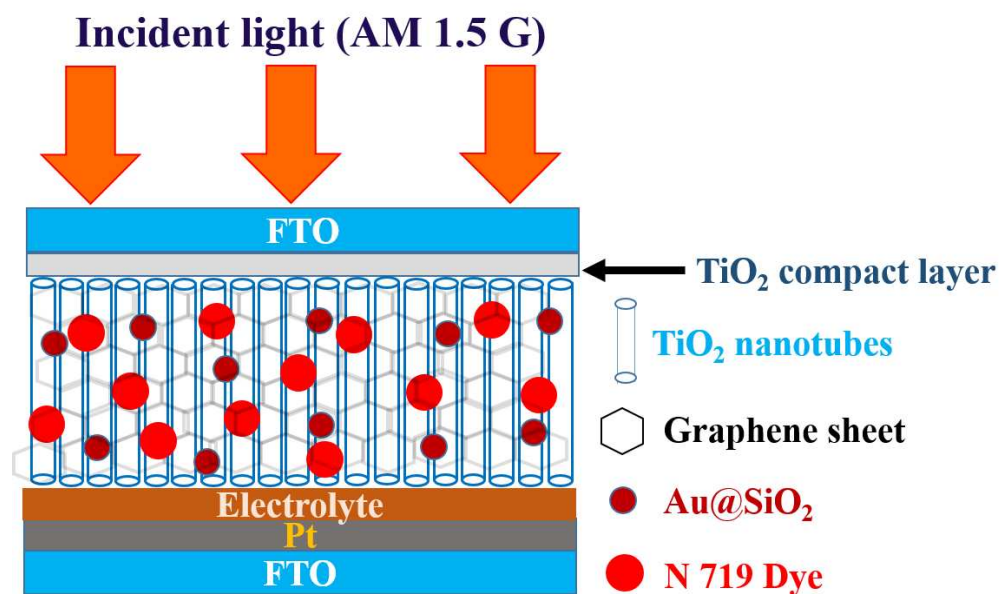
30. M. D. Brown, T. Suteewang, R. Sai santhosh Kumar, V. D'Innocenzo, A. Petrozza, M. M. Lee, U. Wiesnr and H. J. Snaith, *Nano Lett.*, 2011, **11**, 438-445.
31. J. Qi, X. Dang, P. T. Hammond and A. M. Belcher *ACS Nano*, 2011, **5**, 7108-7116.
32. Q. Xu, F. Liu, K. Cui, X. Feng, W. Zhang and Y. Huang, *Sci. Rep.*, 2013, **3**, 2112-2118.
33. S. D. Standridge, G. C. Schatz and J. T. Hupp, *J. Am. Chem. Soc.*, 2009, **131**, 8407-8409.
34. K. Guo, M. Li, Xi. Fang, Xi. Liu, B. Sebo, Y. Zhu, Z. Hu and Xi. Zhao, *J. power sources*, 2013, **230**, 155-160.
35. A. A. Madhavan, R. Ranjusha, K. C. Daya, T. A. Arun, P. Praveen, K. P. Sanosh, K. R. V. Subramanian, S. K. V. Nair, A. S. Nair and A. Balakrishnan, *Sci. Adv. Mater.* 2014, **6**, 1-7.

**Table 1.** Photovoltaic parameters of DSSCs prepared with pristine TNTs, N-TNTs, and graphene/N-TNT composites as photoanodes.

DSSCs	Voc (V)	Jsc (mA/cm <sup>2</sup> )	FF (%)	η (%)	Dye loading (× 10 <sup>-7</sup> mol/cm <sup>2</sup> )
Pristine TNTs	0.681	7.43	72.29	3.86	0.76
N-TNTs	0.696	8.34	73.80	4.29	0.85
0.2wt% G/N-TNTs	0.711	9.60	71.32	4.87	0.92
0.4wt% G/N-TNTs	0.701	11.24	69.29	5.46	1.11
0.6wt% G/N-TNTs	0.718	12.86	68.59	6.33	1.53
0.8wt% G/N-TNTs	0.712	12.25	68.13	5.94	1.29
1.0wt% G/N-TNTs	0.721	11.63	68.55	5.76	1.16

**Table 2.** Photovoltaic parameters of plasmonic-DSSCs prepared with different amounts of Au@SiO<sub>2</sub> core-shell NPs embedded in 0.6wt% graphene/N-TNT composite.

Plasmonic-DSSCs	Voc (V)	Jsc (mA/cm <sup>2</sup> )	FF (%)	η (%)	Dye loading (× 10 <sup>-7</sup> mol/cm <sup>2</sup> )
0.6wt% G/N-TNTs	0.718	12.86	68.59	6.33	1.53
0.6wt% Au@SiO <sub>2</sub>	0.720	13.10	67.78	6.40	1.46
1.2wt% Au@SiO <sub>2</sub>	0.725	14.05	66.08	6.74	1.38
1.8wt% Au@SiO <sub>2</sub>	0.715	15.61	62.77	7.01	1.29
2.4wt% Au@SiO <sub>2</sub>	0.750	13.73	62.96	6.48	1.32



**Scheme 1** Schematic diagramme of DSSC fabricated using N-TNTs mixed with graphene and Au@SiO<sub>2</sub> core-shell NPs.

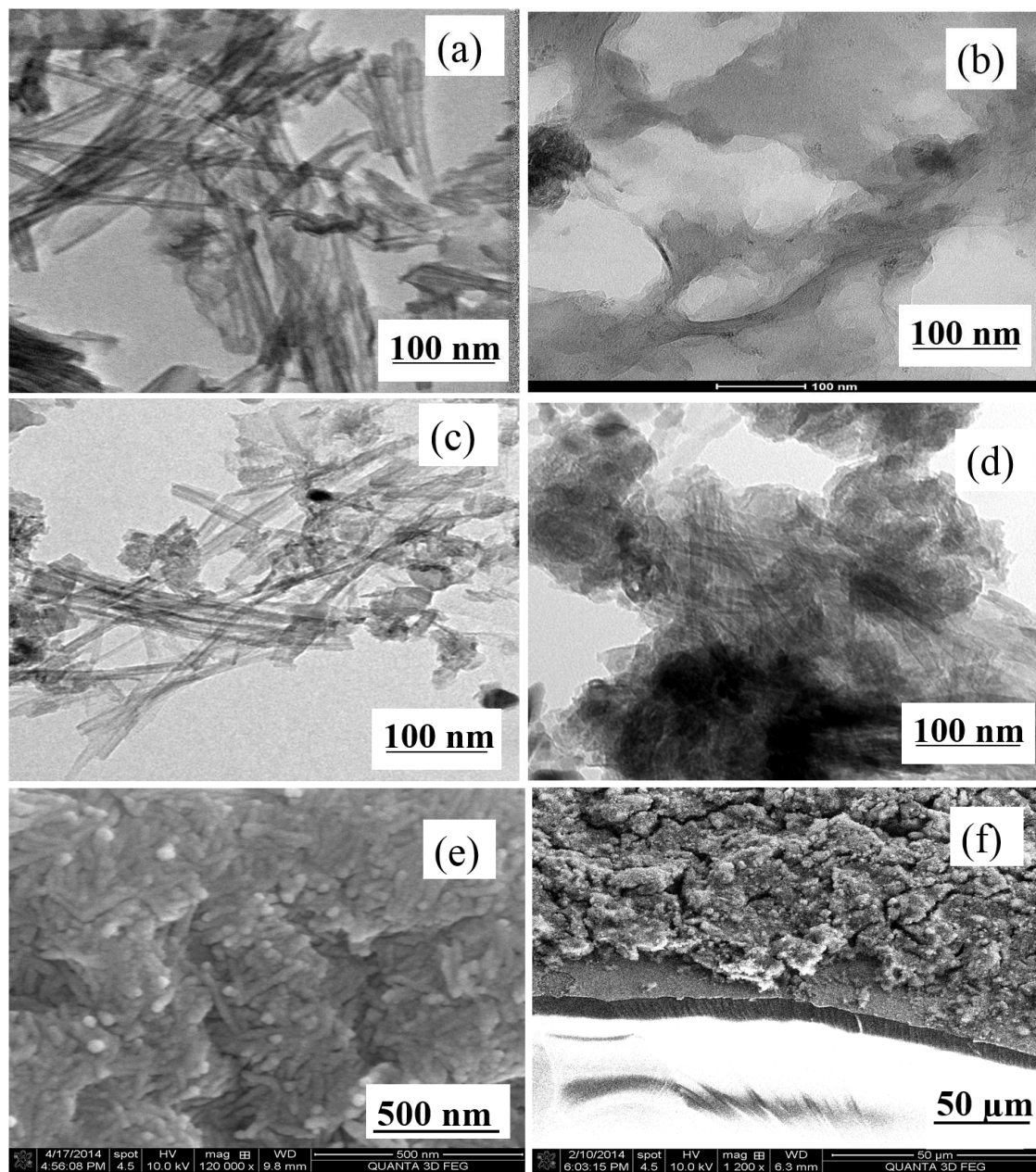


**Fig. 1** TEM images of (a) N-TNTs, (b) graphene sheets, (c) graphene/N-TNT composite with 0.6wt% graphene, and (d) graphene/N-TNT composite with 1.0wt% graphene. SEM images of NC films of (e) N-TNTs and (f) cross sectional view of 0.8wt% graphene/N-TNTs.

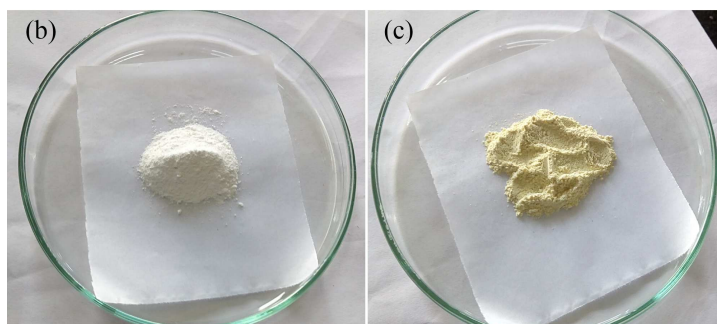
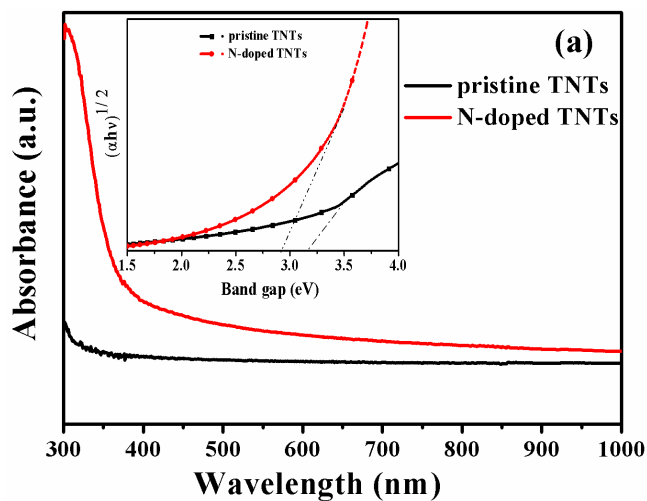


**Fig. 2** (a) UV-Visible absorbance spectra of pristine TNTs and N-doped TNTs, inset of figure shows the band gap variation of TNTs with nitrogen doping, (b) and (c) photographs of as prepared pristine TNTs and N-doped TNTs.

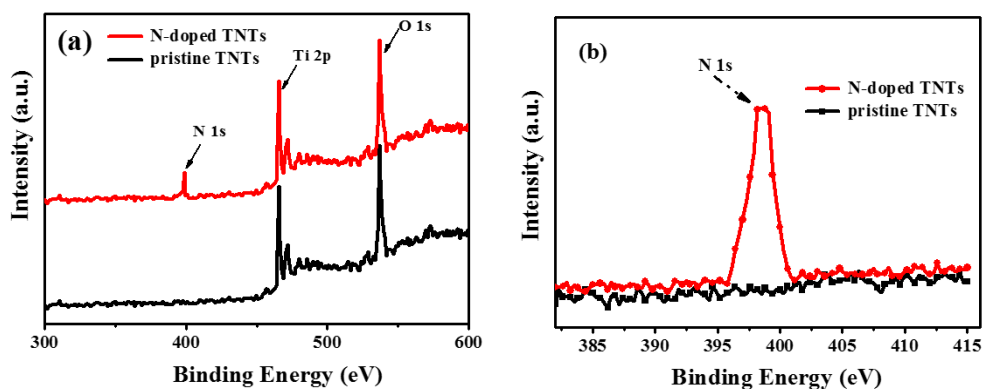


**Fig. 3** (a) Wide scan XPS spectra, and (b) N1s core level spectra of pristine and N-doped TNTs.

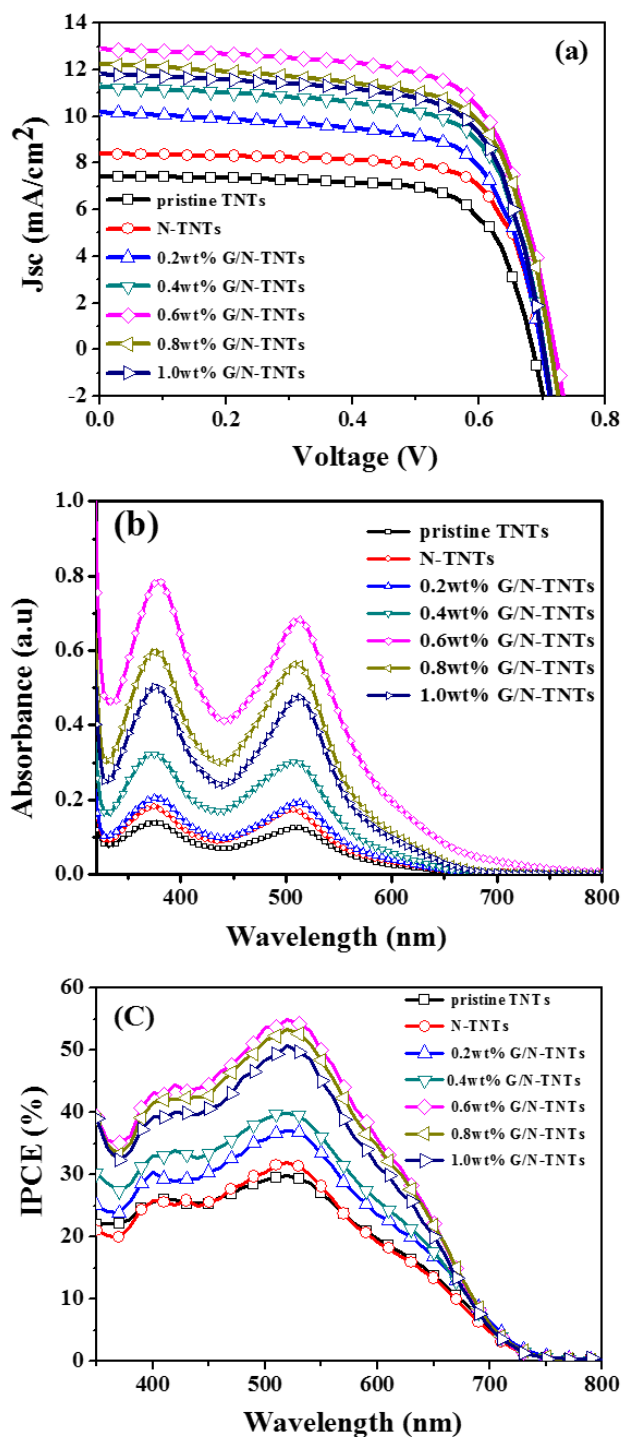


**Fig. 4** (a)  $J$ - $V$  graphs, (b) absorbance spectra of dye desorption, and (c) IPCE spectra of pristine TNTs, N-TNTs and graphene/N-TNT composites with varying concentrations of 0.2, 0.4, 0.6, 0.8, and 1.0 wt. % graphene. (In graphs G means graphene)

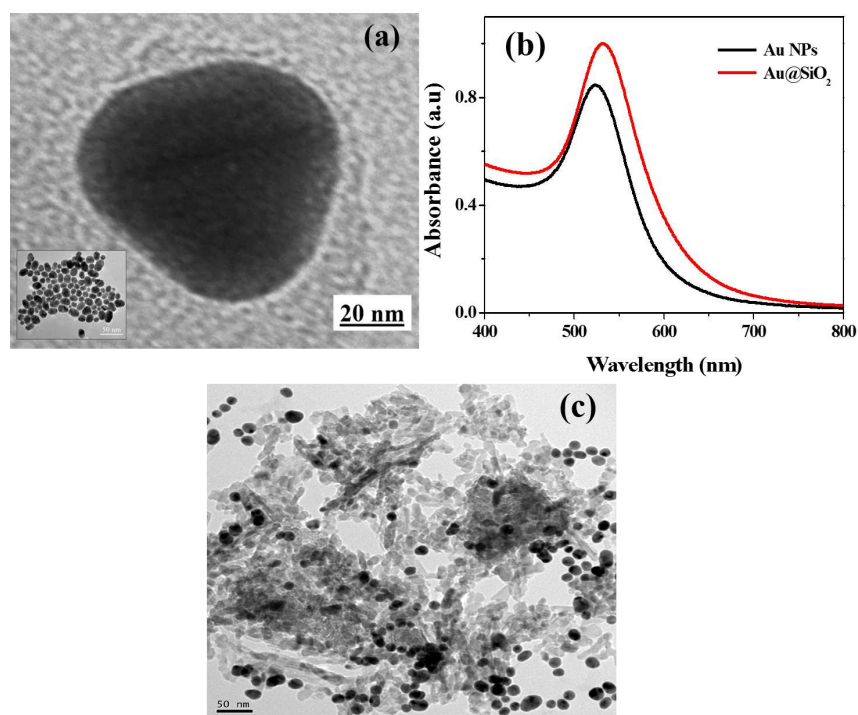


**Fig. 5** (a) TEM image of Au@SiO<sub>2</sub> core-shell NPs, (b) UV-Visible absorbance spectra of Au and Au@SiO<sub>2</sub> core-shell NPs, and (c) TEM image of Au@SiO<sub>2</sub> core-shell NPs embedded in graphene/N-TNTs.

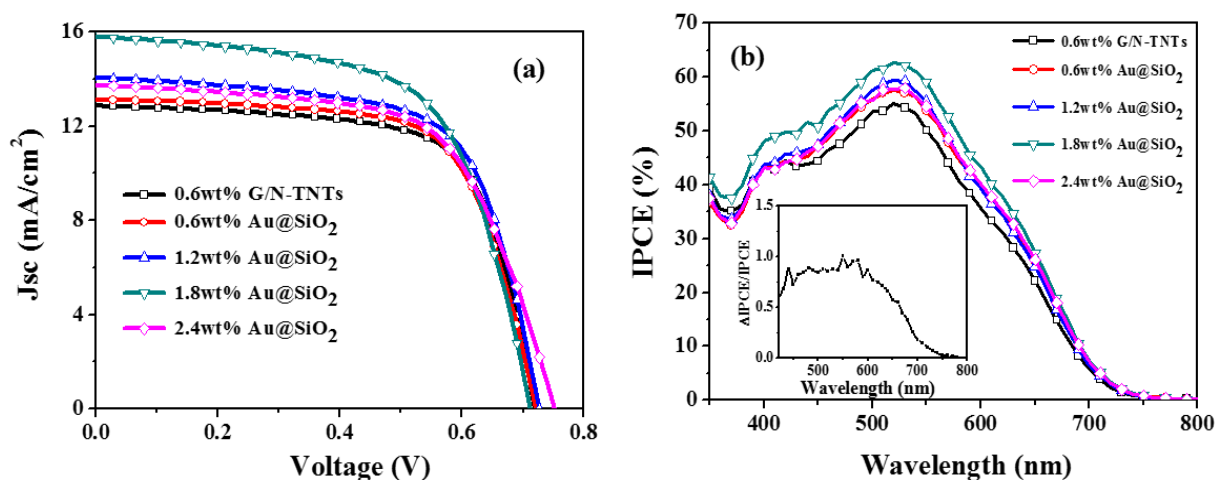


**Fig. 6** (a) J-V graphs and (b) IPCE spectra of DSSCs with varying concentration of 0.6, 1.2, 1.8 and 2.4wt% Au@SiO<sub>2</sub> core-shell NPs embedded in 0.6wt% graphene/N-TNT composite, and an inset shows the relative IPCE enhancement  $[(IPCE_{1.8wt\%Au@SiO_2} - IPCE_{0.6wt\%graphene/N-TNTs})/IPCE_{0.6wt\%graphene/N-TNTs}]$  spectrum. (In graphs G means graphene)

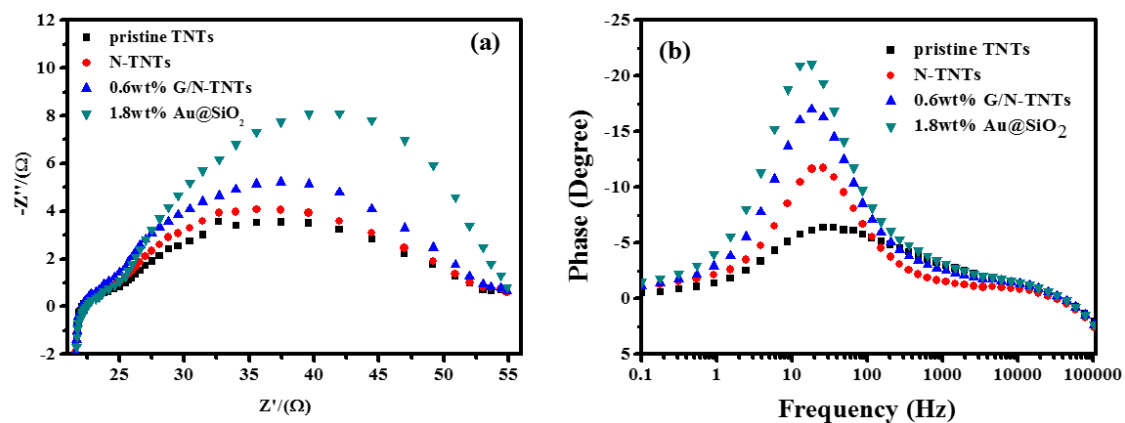


**Fig. 7** (a) Nyquist and (b) Bode plots of DSSCs based on N-TNTs, 0.6wt% graphene/N-TNTs and 1.8wt% Au@SiO<sub>2</sub> core-shell NPs in 0.6wt% graphene/N-TNTs. (In graphs G means graphene)

## Graphical Abstract

